Vol. 429: 29–43, 2011
doi: 10.3354/meps09097

MARINE ECOLOGY PROGRESS SERIES
Mar Ecol Prog Ser

Published May 16

Plankton dynamics in an estuarine plume: a mesocosm ^{13}C and ^{15}N tracer study

Karel Van den Meersche[1,2,3], Karline Soetaert[2,*], Jack J. Middelburg[2,4]

[1]Department of Biology, Marine Biology Section, Ghent University, 9000 Ghent, Belgium
[2]Centre for Estuarine and Marine Ecology, Netherlands Institute of Ecology (NIOO - KNAW), 4400 AC Yerseke, The Netherlands
[3]*Present address:* Eco&Sols, CIRAD, 34060 Montpellier, France
[4]*Present address:* Faculty of Geosciences, Utrecht University, 3508 TA Utrecht, The Netherlands

ABSTRACT: Flows of carbon and nitrogen in a natural phytoplankton assemblage from the plume of the Scheldt estuary were followed during and after a light-induced bloom by measuring changes in concentrations and stable isotope ratios in mesocosms after addition of ^{13}C (as bicarbonate or glucose) and ^{15}N (as ammonium or nitrate). Addition of ^{13}C-bicarbonate showed a strong coupling between algal primary production and bacterial secondary production, while addition of ^{13}C-glucose revealed bacteria as a carbon source for eukaryotes. Tracing the ^{13}C into mesozooplankton, we identified selective grazing on algae during the phytoplankton bloom, transfer of carbon from bacteria to mesozooplankton and opportunistic feeding strategies after the bloom. Nitrogen labeling confirmed carbon labeling findings, identified bacteria rather than mesozooplankton as ammonium regenerators and allowed quantification of nitrification.

KEY WORDS: Plankton · Isotope · Estuarine

INTRODUCTION

While algae are the primary source of new organic carbon in coastal and estuarine ecosystems and, hence, often the main food source for multicellular organisms, bacteria are undeniably key players in the processing and upgrading of detritus (non-living organic material) from terrestrial origins. More specifically, in many tidal estuaries, external organic matter input can be so high that the bacterial community thriving on it exceeds primary producers in productivity and sometimes even biomass. An excellent example is the Scheldt estuary, where a combination of high nutrient concentrations, high particle load and colored dissolved organic matter often causes primary producers in the upper estuarine reaches to be light limited, making the estuary heterotrophic (Heip et al. 1995, Soetaert et al. 2006).

As turbidity decreases downstream, phytoplankton gradually dominates the organic matter pool and the role of bacteria is pushed from processing external organic matter towards regeneration of locally produced algal material (Boschker et al. 2005). A temporary strong coupling between bacterial and algal production can be expected during phytoplankton blooms, when algal exudates become available in large amounts. Bacteria also thrive in the post-bloom phase, when nutrient limitation forces algae to exudate the surplus of photosynthetic products, and algal mortality supplies fresh organic matter to the detritus pool (Anderson & Williams 1998, Van den Meersche et al. 2004).

Heterotrophic bacteria are able to utilize a wide range of substrates and can live upon allochthonous organic matter as well. They can be considered 'upgraders' of organic matter since bacteria can be grazed upon by microzooplankton, which in turn can be consumed by mesozooplankton (Klein Breteler et al. 1999). Moreover, bacteria associated to particles can

*Corresponding author: Email: k.soetaert@nioo.knaw.nl

be ingested directly by mesozooplankton. These pathways of the microbial loop are inefficient and much of the carbon may be lost to respiration. Also, because allochthonous organic matter has lower nutritional value, we can expect that mesozooplankton prefer algae, as has been found in feeding experiments (Tackx et al. 1995). Nevertheless, the microbial loop may still contribute significantly to mesozooplankton production in the lower estuarine reaches because of the large supply of allochthonous organic material.

We used stable isotope tracer experiments to quantify carbon and nitrogen flows in a pelagic microbial food web. The addition of labeled substrates and the subsequent stable isotope analysis of group-specific microbial biomarkers have been shown to enable direct identification of microbes in specific processes, and to allow for the incorporation of bacteria into food web studies (Boschker & Middelburg 2002). Unlike terrestrial ecosystems, sediments or small water bodies, where labeled substrates can be injected directly under field conditions (e.g. Van Oevelen et al. 2006), tracer addition in open pelagic systems demands a mesocosm setup to prevent the tracer from dispersing too quickly (Van den Meersche et al. 2004, De Kluijver et al. 2010). Because of their small scale, simplified, zero-dimensional mechanistic models can be applied to mesocosms in order to quantify ecosystem fluxes.

In this paper, we discuss the outcome of a light-induced diatom bloom in a mesocosm experiment with water from the Scheldt plume. No nutrients were added, as the system is naturally light limited, and nutrient levels were sufficiently high to allow bloom formation. The primary goal was to quantify carbon and nitrogen fluxes between algae, bacteria and consumers; more specifically, carbon coupling between algae and bacteria, and carbon fluxes through the microbial loop. In different replicates, either ^{13}C-bicarbonate and ^{15}N-nitrate or ^{13}C-glucose and ^{15}N-ammonium were added in trace quantities. This multi-labeling approach allowed to simultaneously trace carbon that entered the food web via algae and bacteria, respectively. Carbon uptake in bacteria and phytoplankton was distinguished by measuring ^{13}C-incorporation in phospholipid-derived fatty acids (PLFA) (Boschker & Middelburg 2002). These PLFA occur in high concentrations in cells, are turned over quickly after cell death and are group-specific, allowing for discrimination between bacteria and major algal groups such as diatoms and green algae. PLFA analysis avoids the need to physically isolate algae and bacteria from the bulk organic matter. Unlike in Van den Meersche et al. (2004), where a complex, mechanistic ecosystem model was used for flux estimates, we opted for simple models that focused on one or a few ecosystem processes. This approach allowed for a more profound statistical analysis of the results.

MATERIALS AND METHODS

Experimental setup. On June 4, 2004, ~1 m^3 of estuarine water with a salinity of 28.5 was collected near Vlissingen, The Netherlands, at the mouth of the Scheldt estuary (51° 26′ N, 3° 40′E), at a water depth of 2 m. Within 6 h, the water was transferred to three 200 l tanks in a temperature-controlled room with a regular regime of 8 h dark and 16 h light (100 µmol photons m^{-2} s^{-1} of photosynthetically active radiation at the water surface). Subsequently, the 3 tanks (A, B and C) were incubated for a 10-d period at the *in situ* temperature of 17.5°C. Particles were kept in suspension through constant mixing. At the beginning of the incubation, stable isotope tracers of carbon and nitrogen were added. Replicates A and B received 500 mg of ^{13}C-bicarbonate (99% ^{13}C), causing a concentration increase of 30 µmol C l^{-1} (1.3%) and an increase in δ^{13}C of 1000‰, and 25 mg of ^{15}N-nitrate (98% ^{15}N), increasing the nitrate concentration by 3.5 µmol N l^{-1} > (7%) and the δ^{15}N by 5000‰. Replicate C received 3.25 mg of ^{15}N-ammonium (98% ^{15}N), increasing the ammonium concentration by 0.5 µmol N l^{-1} (over a background concentration of 1 µmol N l^{-1}) and the δ^{15}N of ammonium by >200 000‰. Replicate C also received 80 mg of ^{13}C-glucose (99% ^{13}C), causing a dissolved organic carbon (DOC) concentration increase of 12 µmol C l^{-1} or 8%. The composition of natural, background DOC is not well known; the percentage increase in concentration of the unknown labile DOC fraction was probably much higher. Temperature, oxygen and pH were measured continuously in replicate A. At the injection of isotope labels (time 0) and after 0.5, 1, 2, 3, 4, 5, 7, 9 and 11 d, 5 l of water from the replicate were pre-filtered through an 80 µm net to separate the mesozooplankton fraction and subsequently subsampled for nutrients, dissolved inorganic carbon (DIC) and DOC, suspended matter (SPM) and PLFA determination. Moreover, unfiltered samples were taken each time for microbial cell counts.

Analytical methods. One liter of water was filtered through pre-weighed, pre-combusted Whatman GF/F filters, which were stored at –20°C and later analyzed for particulate nitrogen (PN) and organic carbon (POC), using an elemental analyzer coupled online to a Finnigan Delta S isotope ratio mass spectrometer (EA-IRMS). The same samples were destructed with concentrated HNO_3:HCl (4:1 ratio) using a microwave (CEM, MDS-2000, 630 VA with Advanced Composite Vessels) and analyzed for particulate organic phosphorus (POP) with inductively coupled plasma optical

emission spectrometry (Perkin Elmer, Optima 3300 DV). GF/F filtered water was analyzed for dissolved phosphate, ammonium, nitrate, nitrite and urea by automated colorimetric techniques.

Samples for DIC were collected in headspace vials (50 ml) and preserved with mercury chloride. DIC concentration and and δ^{13}C-DIC were measured using EA-IRMS (Moodley et al. 2000).

Samples for DOC (20 ml) were filtered through pre-combusted GF/F filters, stored frozen and analyzed for concentration and δ^{13}C using a combined UV wet oxidation technique. Briefly, DIC was removed by adding sulphuric acid in excess (0.32 ml 0.5 N H_2SO_4 per 2 ml of sample) and subsequent stripping with He. The samples were analyzed with a Skalar Formacs total organic carbon (TOC) analyser coupled through a Conflo II interface to a Finnigan Delta S IRMS. The calibration standards were prepared with potassium phthalate dissolved in purified water.

The δ^{15}N in NH_4^+ and NO_3^- was measured using a diffusion technique (Andersson et al. 2006); NH_4^+ and subsequently NO_3^- (converted into NH_4^+ using Devarda's alloy) in the sample was trapped on a GF/D filter. The ^{15}N content of the GF/D filters was determined using a Fisons NA 1500 elemental analyzer coupled to a Finnigan Delta S IRMS via a Conflo II interface.

About 2 l of water were filtered through pre-combusted GF/F filters for subsequent measurement of PLFA concentration and isotopic composition. In short, eukaryote and bacterial PLFA were extracted according to Boschker et al. (1999) and Middelburg et al. (2000). Concentrations and δ^{13}C of specific PLFA were measured using gas chromatography-combustion-IRMS (GC-c-IRMS) (Boschker & Middelburg 2002). Eukaryote and bacterial carbon concentrations and δ^{13}C were calculated from the PLFA data as described in Middelburg et al. (2000): From the bacterial PLFA, total bacterial concentration (C_{bact}) can be calculated as:

$$C_{bact} = \frac{\sum PLFA_{bact}}{a} \quad (1)$$

where a is the average PLFA concentration in bacteria (0.073 g C PLFA g^{-1} C biomass for aerobic environments (Brinch-Iversen & King 1990)).

Not all bacterial PLFA are exclusively found in bacteria; thus, Eq. (1) cannot be used as such. Rather, the sum of bacteria-specific PLFA (i14:0, i15:0 and a15:0 and i16:0) is used instead, and it is assumed that this comprises 14% of total PLFA:

$$C_{bact} = \frac{\sum PLFA_{bact,spec}}{a \times b} \quad (2)$$

where b = 0.14 g specific bacterial PLFA g^{-1} bacterial PLFA content (Moodley et al. 2000).

Total concentration of eukaryotic microplankton (C_{MP}) was estimated as:

$$C_{MP} = \frac{\sum PLFA_{MP,spec}}{c} \quad (3)$$

The constant c, the ratio between carbon content of eukaryote-specific PLFA (16:3ω3, 16:3ω4, 16:4ω3, 16:4ω1, 18:3ω3, 18:4ω3, 18:5ω3, 18:5ω[3,6,9,12,16], 20:5ω3, 22:6ω3) and total carbon content (g g^{-1}), was set at c = 0.035 from Day 0 to 4, a value found in diatoms (Middelburg et al. 2000). From Day 5 onward, this value was fixed at c = 0.060, as found in *Phaeocystis* (N. Dijkman pers.comm.). The δ^{13}C of eukaryotes and bacteria were estimated taking the weighted average from the δ^{13}C of their group-specific PLFA and adding an estimated fractionation value of 3 ‰ (Hayes 2001).

Mesozooplankton samples, mainly consisting of copepods, were stored in a freezer immediately upon harvesting. They were subsequently rinsed twice in deionized water, sorted according to genus and size, collected in tin cups and dried at 60°C. Around 5 adult copepods were collected per tin cup for δ^{13}C analysis, and ~30 adults per tin cup for δ^{15}N. More individuals were used for smaller organisms. The cups were later analyzed for δ^{13}C and δ^{15}N using EA-IRMS.

Microbial cell counts. Cell counts were performed to compare dynamics of heterotrophic and autotrophic eukaryotic cells and bacterial cells, and to confirm the results obtained from lipid analysis. Between 30 and 50 ml of water were filtered over 0.45 µm polycarbonate membrane filters and colored with Primulin, then studied under a microscope with UV light. We discriminated between autotrophic and heterotrophic cells based on fluorescence. Autotrophic cells were subdivided in diatoms, *Phaeocystis* and other. For bacterial counts, unfiltered water samples were fixed with 4% formalin and kept at 4°C. They were diluted 10 to 20 times with a Trizma/EDTA buffer of pH 8, colored with Sybrgreen to an end concentration of 100 µl l^{-1}and subsequently analyzed on a Coulter Elite Flow Cytometer with an excitation 488 nm laser of 20 mW. Emission was measured in the 510 nm channel with the photomultiplyer at 600.

Models. Carbon uptake rates were investigated in a series of simple food web models with similar structure. The main flow schemes are depicted in Fig. 1, and detailed model formulations are represented in Appendix 1. The models are built around mass balance equations of the form:

$$\frac{dC_X}{dt} = \sum \text{Uptakes} - \sum \text{Losses} \quad (4)$$

and stable isotope equations of the form:

$$\frac{d\delta^{13}C_X}{dt} = \sum_{i \text{ in Sources}} (\delta^{13}C_i - \delta^{13}C_X) \times \nu_i, \text{ with } \nu_i = \frac{\text{Uptake}_i}{C_X} \quad (5)$$

where C_X is carbon concentration of the consumer, $\delta^{13}C_X$ is the carbon isotope ratio in the consumer and $\delta^{13}C_i$ is the carbon isotope ratio in source component i. This formulation assumes the isotope ratio not to be affected by loss processes, which is correct only if losses operate on bulk tissue, and there is no fractionation during trophic transfers. Fractionation effects can be neglected in highly enriched samples, as is the case in this study.

The simplest model (Model I, Fig. 1a) describes primary production as a constant flux of carbon from the DIC pool to eukaryotic microplankton (MP). MP consists mainly of algae and its concentration, and isotope compositions are estimated from eukaryotic PLFA. Eq. (4) then becomes:

$$\frac{d\delta^{13}C_{MP}}{dt} = (\delta^{13}C_{DIC} - \delta^{13}C_{MP}) \times \frac{PP}{C_{MP}} = (\delta^{13}C_{DIC} - \delta^{13}C_{MP}) \times \nu_{PP} \quad (6)$$

where the microplankton growth rate, $\nu_{PP} = \frac{PP}{C_{MP}}$, is the estimated parameter. PP (primary production, µmol C l^{-1} d^{-1}) is restricted to the production of algal biomass, excluding exudates and algal respiration, and ν_{pp} can be calculated for every timestep by differentiating

$$\left(\frac{d\delta^{13}C}{dt} \approx \frac{\delta^{13}C_{t+\Delta t} - \delta^{13}C_t}{\Delta t}\right) \text{and then solving Eq. (6).}$$

Model II (Fig. 1b) estimates the exudation of DOC compounds by algae and their subsequent uptake by bacteria. DOC exudation is modeled as a carbon flux from DIC to DOC, which varies linearly with the concentration of MP (rate parameter ν_{Ex}, see Appendix 1). This new, exudated DOC is supposed to be readily taken up by bacteria, and is thus referred to in the model as labile DOC (LabDOC). Bacteria have then the choice between uptake of this labile, ^{13}C-enriched LabDOC produced by algae, or non-labeled DOC, with a low, natural abundance $\delta^{13}C$. Uptake rates take into account a Monod-type response to the substrate concentrations. Bacteria, labile DOC and their respective isotope ratios are implemented as dependent variables (i.e. they are dynamically described), while the rest are independent variables (i.e. they are imposed upon the model as forcing functions).

Microzooplankton grazing on bacteria is estimated with a model that includes 3 fluxes into MP: primary production, microzooplankton grazing on bacteria (G) and direct uptake of glucose (MGU) (Model III, Fig. 1c; see Appendix 1). Primary production is modeled in the same way as in Model I; MGU has a Monod response to the (quickly depleted) glucose concentration (parameter k_{GU}). Both the results from the DIC labeling (replicates A and B) and the glucose labeling (replicate C) are used in this model. $\delta^{13}C$ of DIC in the bicarbonate-labeled replicates (A, B) and $\delta^{13}C$ of bacteria in the glucose-labeled treatment (C) are used as independent variables, while $\delta^{13}C$ of DIC in the glucose-labeled treatment and $\delta^{13}C$ of MP are the dependent variables.

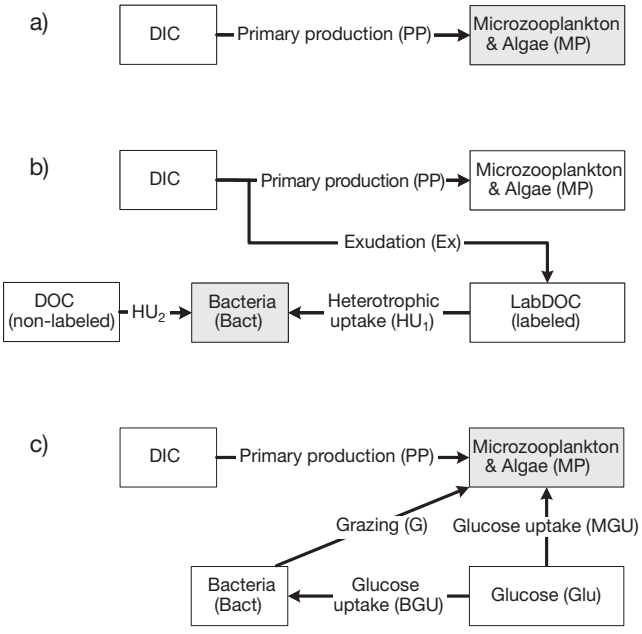

Fig. 1. Model schemes for carbon flows: Models (a) I, (b) II, (c) III. Grey boxes: compartments fitted to data. See Appendix 1 for model equations. DOC/DIC: dissolved organic/inorganic C

Models II and III were implemented in the R software (R development core team, 2010) and integrated using the R package deSolve (Soetaert et al. 2010). A Bayesian approach with an adaptive Metropolis-Hastings algorithm, implemented in package FME (Soetaert & Petzoldt 2010), was used to fit the model to the data and estimate parameter probability distributions.

Nitrification was estimated from the temporal evolution of $\delta^{15}N$ of nitrate ($\delta^{15}NO_3$) after addition of labeled ammonium in replicate C. $\delta^{15}NO_3$ in replicate C showed an approximately linear increase during the experiment, indicating that $d\delta^{15}NO_3/dt$ was approximately constant. Consequently, $d\delta^{15}NO_3/dt$ was calculated from the slope of a regression line through the $\delta^{15}NO_3$ data. Nitrification was then calculated using the appropriate interpretation of Eq. (4):

$$\frac{d\delta^{15}NO_3}{dt} = (\delta^{15}NH_4 - \delta^{15}NO_3) \times \frac{nitrification}{[NO_3]} \quad (7)$$

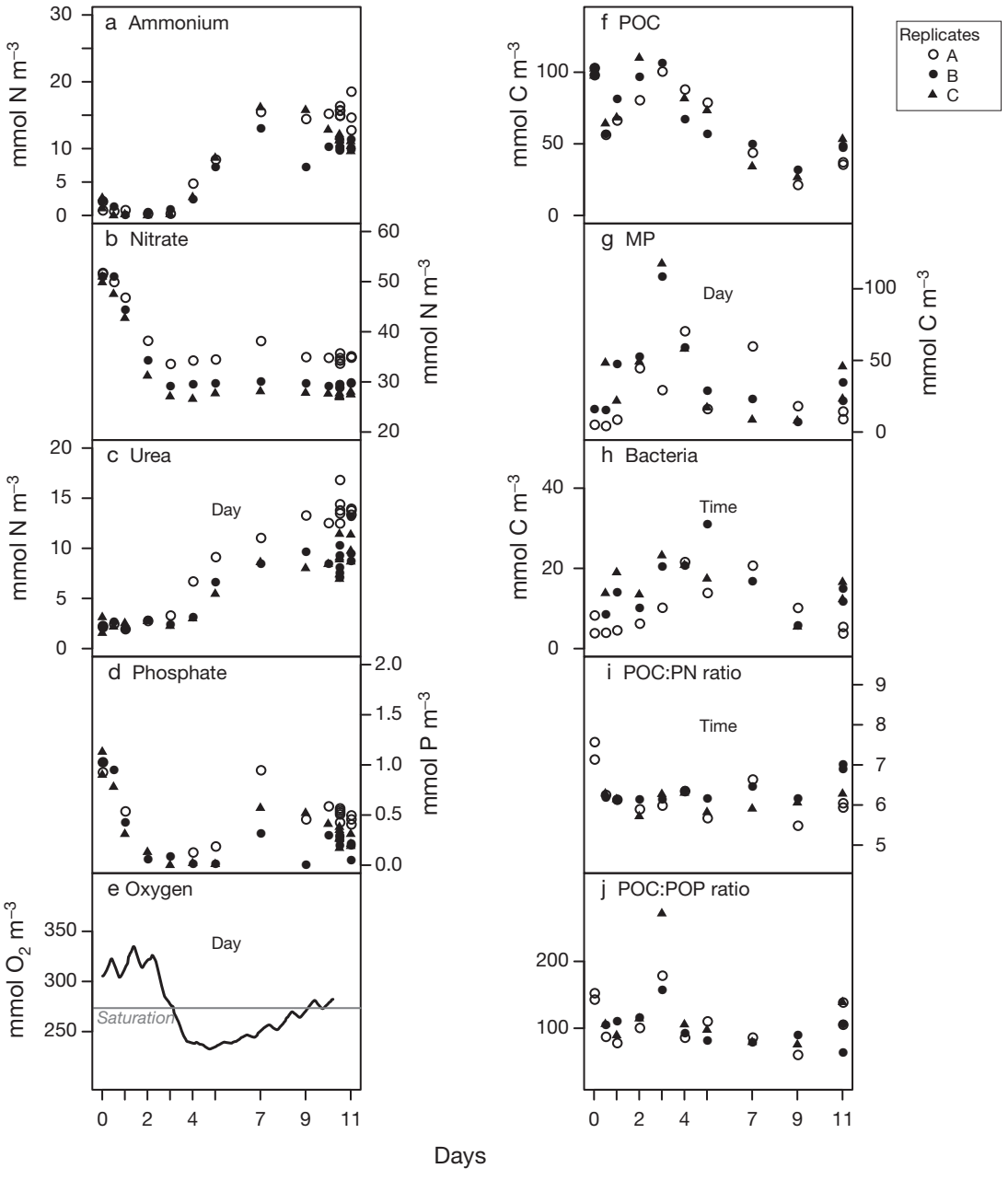

Fig. 2. Concentrations of (a–d) nutrients, (e) oxygen and (f) particulate organic carbon (POC); biomass of (g) eukaryotic microplankton (MP) and (h) bacteria; and (i,j) POC:PN and POC:POP ratios during incubations in the 3 mesocoms. PN: particulate nitrogen; POP: particulate organic phosphorus

RESULTS

Nutrients and particulate matter

The 3 enclosures exhibited similar temporal behavior and will therefore be considered replicates (Fig. 2). Initially, there were high background nutrient concentrations, typical for the highly eutrophied Scheldt estuary: ammonium and nitrate concentrations were 4 and 50 µmol l^{-1}, respectively (Fig. 2a,b). Phosphate concentrations were 1 µmol l^{-1} (Fig. 2d). The high initial background concentration of DIC (~2.2 mmol C l^{-1}, data not shown) was maintained throughout the experiment, with small variations mirroring POC concentrations. The initial pH of 8.2 decreased slightly over the course of the experiment to 8.0 (not shown). Based on changes in nutrient and particulate matter concentrations, 4 phases could be distinguished: an exponential growth phase with the development of a diatom bloom (Phase 1: Days 0 to 2), unbalanced growth under P-lim-

itation (Phase 2: Days 2 to 4), collapse of the bloom with a heterotrophic phase and nutrient regeneration (Phase 3: Days 4 to 7), and a phytoplankton recovery phase (Phase 4: Days 7 to 11).

At the start of the incubation, a diatom bloom was initiated because of improved light conditions. The algae depleted ammonium within 1 d (Fig. 2a), subsequently using nitrate as a nitrogen source. Phosphate was depleted within 2 d (Fig. 2d), but nitrate concentrations continued to decrease (Fig. 2b). At the same time, concentrations of POC and PN kept rising until Day 3 (Fig. 2f,i), thus suggesting decoupling of phosphate uptake from carbon fixation and nitrogen uptake. This can also be concluded from the trends in the C:N and C:P ratios of SPM: the C:N ratio remained fairly constant around the Redfield ratio (106:16) (Fig. 2i), while the C:P ratio peaked at Day 3 to an average of 200:1, almost double the ratio before and after that day (Fig. 2j).

At Day 4, the diatom bloom collapsed and particulate organic carbon and nitrogen declined. Nitrate concentrations stabilized at ~30 µmol l^{-1} and phosphate remained depleted (Fig. 2b,d). Oxygen concentrations reached a minimum of 80% saturation (Fig. 2e). Notwithstanding these high oxygen concentrations, ammonium regeneration led to ammonium concentrations well above pre-bloom levels (Fig. 2a). A subsequent regeneration of phosphate announced the start of a fourth phase (Fig. 2f). A *Phaeocystis* bloom arose, with increasing dissolved oxygen and POC and PN concentrations as a result (Fig. 2e,f,i).

Note the gap in the P and N budgets: the sum of dissolved inorganic nitrogen (DIN) (NH_4^+, NO_3^-, NO_2^-), urea and PN decreased from 70 µmol N l^{-1} at the beginning of the experiment to 50 µmol N l^{-1} at Day 4, and recovered only partly during Phases 3 and 4, reaching values of ~60 µmol N l^{-1}. The sum of POP and dissolved inorganic P declined from 1.5 µmol P l^{-1} to 0.8 µmol P l^{-1} at Day 4, and remained <1 µmol P l^{-1} for the rest of the experiment. The POC:POP ratio quickly returned to values close to or slightly below the Redfield ratio (106:1; Fig. 2j), while inorganic phosphate concentrations remained low. We did not observe settling of algae on the bottom of the tanks, and any effects of such settling were minimized by thorough mixing prior to sampling. Dissolved organic nitrogen (DON) and phosphorus (DOP) may be the missing links in respectively the N and P budgets.

Microbial community

Cell counts (data not shown) showed diatoms to be dominant during Phase 1 and 2; heterotrophic cells dominated the eukaryotic community in Phase 3, while *Phaeocystis* proliferated during Phase 4. Bacterial counts were also highest in Phase 3. It is not clear whether the heterotrophs (microzooplankton and copepods) in Phase 3 contributed to the diatom bloom collapse at the transition of Phase 2 to 3.

Eukarytoic and bacterial concentrations calculated from PLFA (Fig. 2g,h) confirmed the microsopic observations: a phytoplankton bloom with maximum at Day 3 (Phase 2), a peak in bacterial biomass in Days 4 and 5 (Phase 3) and partial recovery of phytoplankton in the final stages.

Mesozooplankton

The mesozooplankton community consisted mainly of calanoid copepods, among which *Temora longicornis* and *Centropages* sp. (only identified up to genus level) were the most abundant (data not shown). Other regularly found genera were *Acartia* and *Pseudocalanus.* Only adult stages of *T. longicornis* and *Centropages* sp. had enough biomass for isotope analysis, and these results are presented further.

The abundance of *Temora longicornis* in the samples increased from 5 to 15 adults l^{-1} in Phase 1 and 2 and declined to 5 adults l^{-1} towards the end of the experiment, trends which can be attributed to food limitation. The abundance of *Centropages* sp. started off at 2 adults l^{-1} and increased gradually to 4 adults l^{-1} at the end of the experiment.

Stable isotope data

Errors on the isotope ratio measurements were determined by taking replicate samples within the replicate incubations at the beginning and the end of the experiment. These were <1‰ for unlabeled compartments, and <10% of the maximum observed increase in $\delta^{13}C$ and $\delta^{15}N$ values instrongly labeled compartments (data not shown). They were generally small compared to variation between replicates. The results of isotope analysis are shown in Fig. 3 and can be divided into 4 subsections: bicarbonate labeling (Fig. 3a–c), glucose labeling (Fig. 3f–h), nitrate labeling (Fig. 3d,e) and ammonium labeling (Fig. 3i,j).

Coupling between algae and bacteria: the bicarbonate labeling experiment

After adding ^{13}C-bicarbonate to replicates A and B, the $\delta^{13}C$-POC increased until Phase 2, when the phytoplankton bloom reached a maximum (Fig. 3a). $\delta^{13}C$-POC never reached the same level as in DIC, and

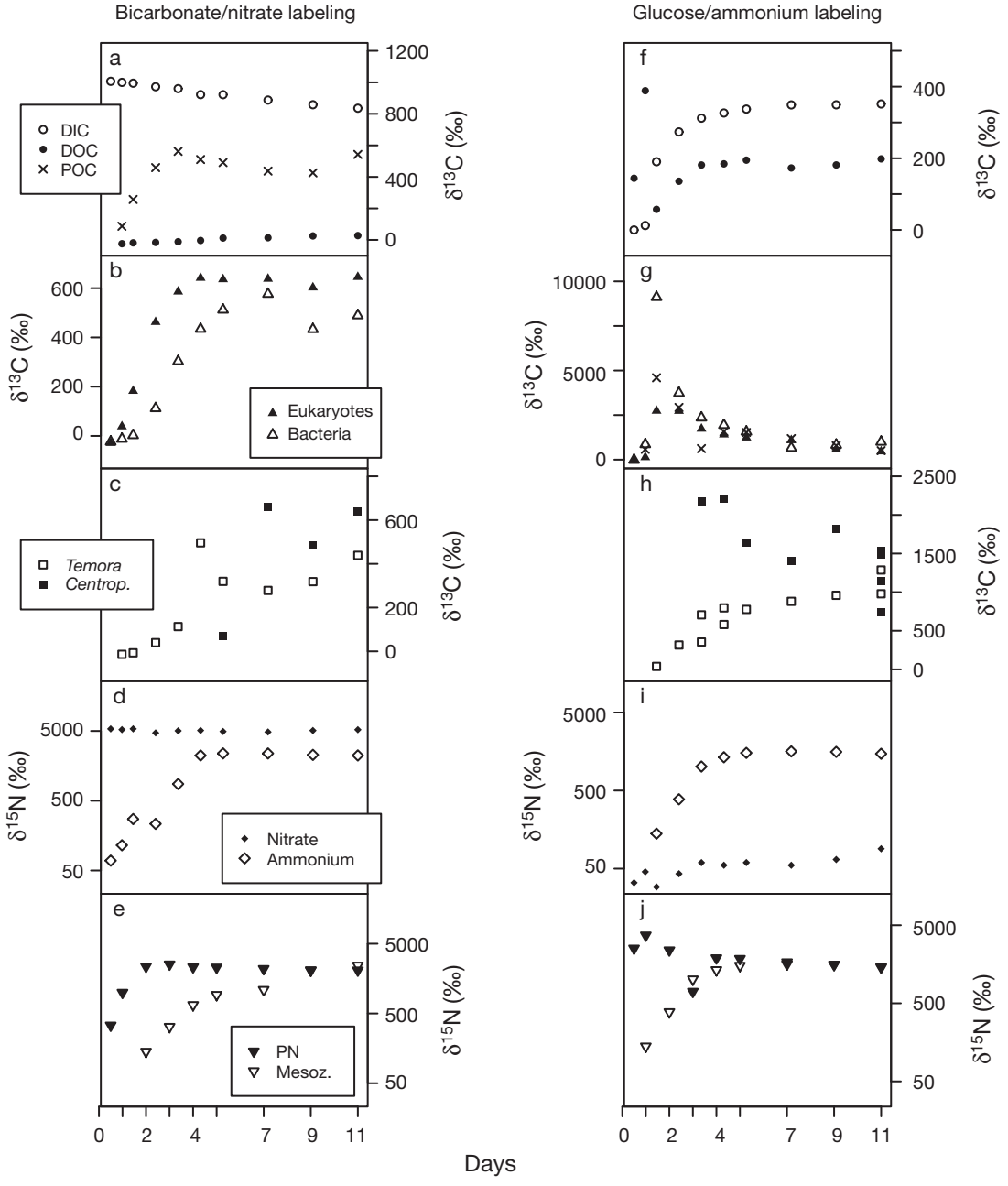

Fig. 3. Carbon labeling patterns after addition of (a–c) ^{13}C-labeled bicarbonate (replicates A and B averaged), or (f–h) ^{13}C-labeled glucose. Nitrogen labeling patterns after addition of (d,e) ^{15}N-nitrate or (i,j) ^{15}N-ammonium. Symbols in the right column of the figure correspond to those in the left column. DIC: dissolved inorganic carbon; DOC dissolved organic carbon; POC: particulate organic carbon; PN: particulate nitrogen. *Centrop*: *Centropages; Temora*: *Temora longicornis*; Mesoz: mesozoplankton

started to decline in Phase 2. This decrease indicates either increased heterotrophic uptake from the unlabeled DOC pool, or selective disappearance of highly labeled material (algae and algal detritus) from the POC pool. The latter may be caused by selective grazing by copepods, or higher degradability of the fresh compared to the refractory organic matter. There was also a steady transfer of ^{13}C to the DOC pool. From a linearization of this transfer, accumulation of recently fixed carbon in the DOC pool was estimated at 1.22 ± 0.16 mmol m^{-3} d^{-1}.

Distribution of label between bacteria and eukaryotes was unraveled with group-specific PLFA. Eukaryote-specific PLFA picked up label almost instanta-

neously, while branched, bacteria-specific PLFA lagged behind by about 2 d (Fig. 3b). The fast uptake of bicarbonate label in eukaryote-specific PLFA reflects primary production, while the delayed appearance in branched PLFA indicates bacterial secondary production on algal derived material (exudates or lysis products).

As in Phase 4, the stable isotope signatures had reached a plateau; an isotope mixing model could be applied, expressing the stable isotopic signature of bacteria as a weighted average of the labeled and unlabeled sources:

$$\delta_{Bact} = p \cdot \delta_{DIC} + (1-p) \cdot \delta_{unlabeled} \quad (8)$$

where, from this model, the fraction of bacterial carbon (p) that comes directly or indirectly from (labeled) DIC could be estimated by:

$$p = \Delta\delta_{Bact} / \Delta\delta_{DIC} \quad (9)$$

where $\Delta\delta = \delta_{enriched} - \delta_{unlabeled}$ is the specific enrichment for each compartment. With p = 58%, this implies that most of the bacterial carbon biomass at the end of the experiment was derived from algae and their exudates.

Heterotrophic pathways and mesozooplankton grazing

The glucose concentration in the third replicate, naturally ~0.05 µmol C l^{-1} (Billen et al. 1980), increased dramatically at the start of the experiment (12 µmol C l^{-1} added), but after 1 d, 60% of the labeled glucose was respired and appeared in the DIC pool, and 40% was incorporated in particulate carbon, mostly bacteria (Fig. 3f,g). A fast initial label uptake was also observed in the lipids 16:4ω3, a biomarker abundant in Chlorophyceae, and 20:5ω3, a biomarker abundant in diatoms, suggesting direct glucose uptake by these groups (not shown). However, the ^{13}C uptake in other eukaryotic PLFA and the average ^{13}C uptake in eukaryotic PLFA showed a delay compared to appearance of ^{13}C in bacterial, branched PLFA (Fig. 3g). This delay in ^{13}C appearance in eukaryotic biomarkers indicates indirect uptake of ^{13}C through microzooplankton grazing on bacteria. Significant label transfer via primary production is ruled out because the $\delta^{13}C$ of DIC was much lower than that of PLFA. These uptake patterns are explored further using the results of Model III.

To assess mesozooplankton grazing, we explore $\delta^{13}C$ data of the 2 main species of mesozooplankton: *Temora longicornis* and *Centropages* sp. (Fig. 3c,h). The transfer of ^{13}C from bicarbonate via phytoplankton to *T. longicornis* was delayed and more gradual than to heterotrophic bacteria (Fig. 3b,c). Maximum enrichment of *T. longicornis* was observed at Day 4 (500‰) and was similar to that of bulk POC (510‰), but higher than that of bacteria at that time (430‰). This indicates that during the bloom, *T. longicornis* acquired most of its ^{13}C from algae. This changed abruptly after the bloom: from Day 4, *T. longicornis* $\delta^{13}C$ decreased in replicates A and B, which can only be explained by a switch to non-labeled food sources, being allochthonous detritus or carbon fixed prior to incubation and the associated microbial food web. After Day 7, when algae became available as a food source once more, the $\delta^{13}C$ increased again.

In contrast, adults of *Centropages* sp. showed a very distinct pattern. Despite the limited amount of data (some missing data points due to insufficient individuals for isotope analysis), an extra delay can be seen in the uptake of label after bicarbonate labeling, suggesting that *Centropages* sp. depended on consumers that feed themselves on algae rather than using algae directly as a food source. This is even clearer from the glucose labeling experiment (Fig. 3h). The high $\delta^{13}C$ values of *Centropages* sp. at Day 4 point to bacteria and microzooplankton as food sources, while the slow uptake of label in *Temora longicornis* confirms an algal diet. After Day 4, $\delta^{13}C$ of *Centropages* sp. gradually diluted towards the signature of bulk POC and bacteria.

Nitrogen isotopes

Labeling patterns for PN, mesozooplankton and ammonium were rather similar irrespective whether ^{15}N-nitrate or ^{15}N-ammonium was added (Fig. 3d,e,i,j). Ammonium and nitrate concentrations (Fig. 2a,b) showed a strong ammonium uptake the first day, followed by nitrate uptake. This explains the small delay observed between the PN labeling patterns following ^{15}N-nitrate compared to ^{15}N-ammonium additions (Fig. 3e,j, respectively). Labeling of mesozooplankton clearly lagged behind that of PN, confirming the microbial community as the prime consumer of inorganic nitrogen (Fig. 3e,j). However, labeling patterns of ammonium (Fig. 3d,i) were due to regenerated ammonium, even for the ammonium addition experiments, because all initial ammonium was consumed within 2 d (Fig. 2a). Ammonium $\delta^{15}N$ lagged behind PN, but was at any time higher than the ^{15}N of mesozooplankton. This points to micro-organisms being the principal source of regenerated ammonium, mesozooplankton having a smaller contribution.

A regression of $\delta^{15}N$-nitrate over time (Eq. 7) after the addition of ^{15}N labeled ammonium led to an estimated nitrification rate of 0.05 ± 0.03 µmol N l^{-1} d^{-1}.

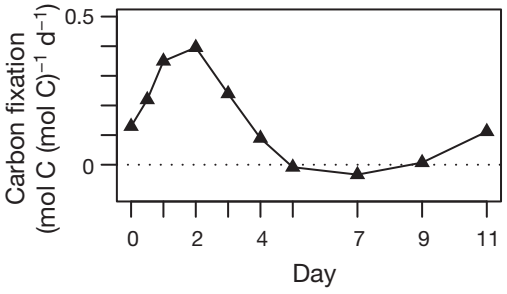

Fig. 4. Net algal carbon fixation (particulate fraction only), calculated from the ^{13}C budget (Model I)

Model results

The net phytoplankton growth rate calculated with Model I (ν_{pp}) increases from 0.1 to 0.5 d^{-1} in the exponential growth phase, to decline to zero in Phase 2. In Phase 3, phytoplankton growth is even slightly negative, to rise again to 0.1 d^{-1} in Phase 4 (Fig. 4).

The results of Model II are shown in Fig. 5a–f, and fitted parameters are in Table 1. The model fitted the bacterial biomass and isotope data reasonably well (Fig. 5a,d). The results showed bacteria to have greater affinity for algal exudates than for allochthonous DOC: the maximum uptake rate for labile DOC, $\nu_{HU1} \approx 6.5$ d^{-1}, was larger than the value for refractory DOC compounds, $\nu_{HU2} \approx 3.8$ d^{-1} (Table 1). However, the realized uptake rate of algal exudates, averaged over a 10-d period, was more in the order of 3.0 d^{-1}, due to limited supply of algal exudates near the end of the experiment (Fig. 5b). As a result, the realized uptake of labile and refractory DOC were of comparable size (Fig. 5e,f). Another noteworthy result of the model is the importance of algal exudates production in relation to primary production: despite the uncertainty in algal exudation rate ($\nu_{Ex} \approx 1.2 \pm 0.3$ d^{-1}), it appears to be very large in comparison with the net production of (particulate) algal biomass (at most 0.4 d^{-1}; see Fig. 4).

Model fits for Model III were also good (Fig. 5g–i). The results for the fitted parameters are in Table 1 and corroborate the previous findings: uptake of glucose by eukaryotes is ~5 times lower than bacterial glucose uptake. The primary production rate, treated as a constant over the course of the experiment in Model III, corresponds well with the results of Model I ($\nu_{PP} \approx 0.3 \pm 0.1$ d^{-1}). Comparing this with $\nu_{Ex} \approx 1.2 \pm 0.3$, we can conclude that 80% of the carbon fixed was exudated.

Model analysis identified microzooplankton grazing on bacteria as an important process (Fig. 5j), but the large uncertainties make it difficult to quantify it with reasonable precision. The Bayesian approach revealed a strong correlation (r = 0.64) between the grazing constant ν_G and bacterial growth efficiency (μ_{Bact}; see Appendix 1) indicating that the model was poorly constrained for these parameters; detailed knowledge of μ_{Bact} would enable to pin down the grazing rate more precisely. A comparison of Figs. 4 & 5j makes it clear that grazing is high, in the same order of magnitude as the net primary production.

DISCUSSION

Stable isotope tracers were introduced as a means to elucidate and quantify carbon and nutrient fluxes in pelagic food webs, more specifically during and after a phytoplankton bloom. Whereas whole system labelling has been applied in sediments (Van Oevelen et al. 2006, Evrard et al. 2010) or in lakes (Pace et al. 2007), this is difficult to achieve in a system that is subject to large exchanges as in the Scheldt estuary. To prevent too high losses of the tracers by mixing processes, we opted for the use of mesocosm experiments, in which exchange with the surroundings is absent. However, there are a few concerns when using mesocosms (e.g. Berg et al. 1999). Firstly, there may be interactions with the enclosure walls. The mesocosms were regularly monitored for any fouling, and none was observed during the course of the experiment. Another potential disadvantage is that any stratification or exchange with sediments is not included. This limits the possibility to translate our results to the field. On the positive side,

Table 1. Carbon model parameter estimates, means and SD (Models II & III). DOC: dissolved organic carbon; PP: primary production

Parameter	Mean	SD	Model	Description	Unit
ν_{Ex}	1.2	0.3	II	DOC exudation rate	mol C (mol C_{MP})$^{-1}$ d^{-1}
ν_{HU1}	6.5	1.2	II	Maximum uptake rate of labeled (fresh) DOC by bacteria	mol C (mol C_{Bact})$^{-1}$ d^{-1}
ν_{HU2}	3.8	0.9	II	Uptake rate of unlabeled (refractory) DOC by bacteria	mol C (mol C_{Bact})$^{-1}$ d^{-1}
ν_{PP}	0.28	0.07	III	Net eukaryote growth rate (PP – exudation – respiration)	mol C (mol C_{MP})$^{-1}$ d^{-1}
ν_{MGU}	4.7	3.5	III	Eukaryotic maximum glucose uptake rate	mol C (mol C_{MP})$^{-1}$ d^{-1}
ν_{BGU}	34.3	20.4	III	Bacterial maximum glucose uptake rate	mol C (mol C_{Bact})$^{-1}$ d^{-1}
ν_G	0.08	0.04	III	Quadratic grazing constant	mol C (mol C_{MP})$^{-2}$ d^{-1}

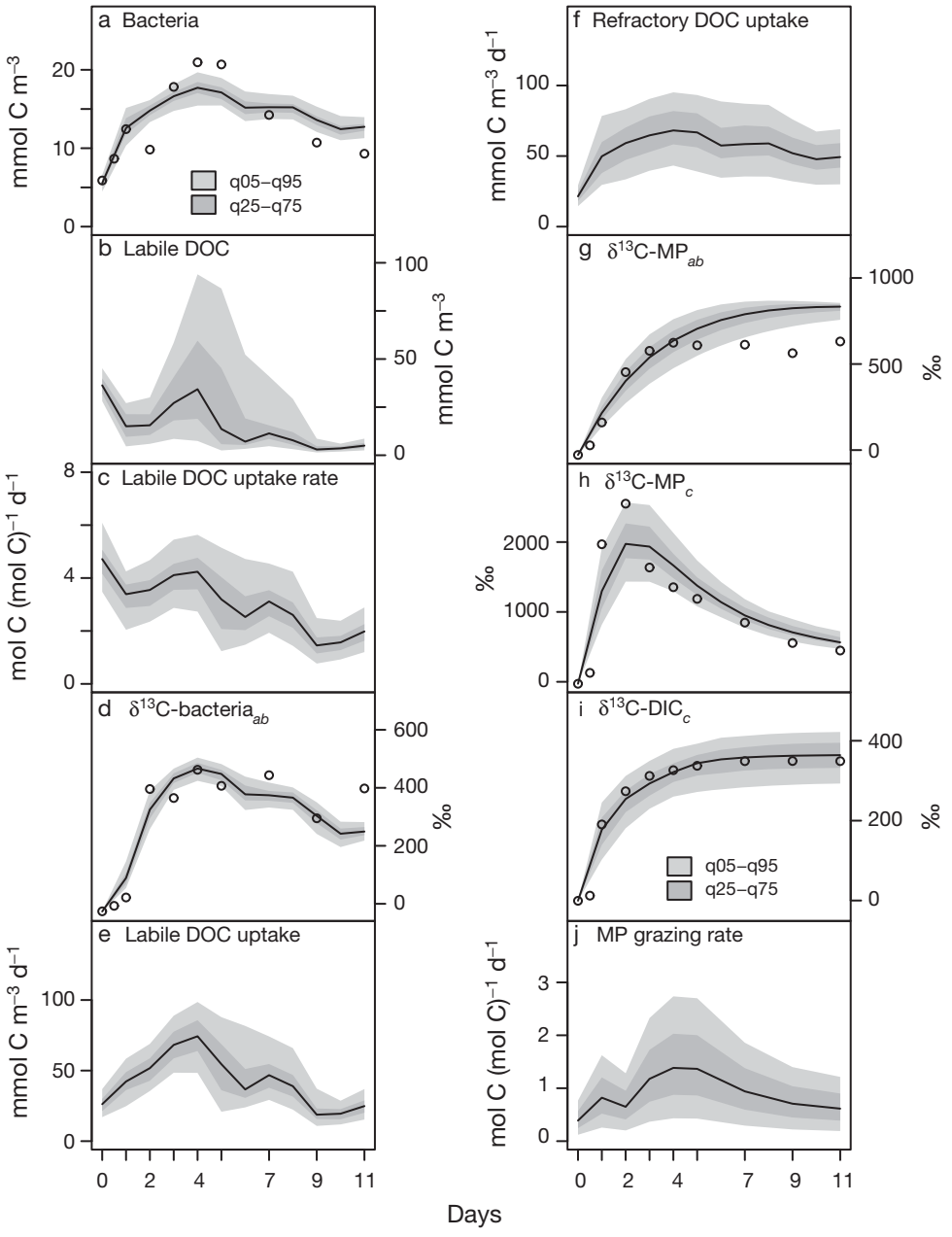

Fig. 5. Dynamic output for Models II (a–f) and) III (g–j). Thick line: best-fit model result. Light grey area: 5 and 95% quantiles (q05–q95). Dark grey area: 25 and 75% quantiles (q25–q75). Quantiles are generated based on the parameter probability intervals. DOC: dissolved organic carbon; DIC: dissolved organic carbon. MP: microplankton

the exclusion of sediments, currents and tides simplifies the system, allowing for direct assessment of stock changes, tracer turnover and mass balances without having to take into account these confounding factors. Also, the data obtained can be easily analysed with simple, zero-dimensional models.

Primary production in the upstream reaches of the Scheldt estuary is mostly light limited (Kromkamp et al. 1995). Going downstream, turbidity decreases and algae grow until they become nutrient limited. We induced the switch from light to nutrient limitation by reducing the mixing depth, thus manipulating the light, without addition of nutrients. The obtained change is more abrupt than occurs under natural conditions, partly because there was no dilution of the nutrients as in the estuary. We therefore expect the estimated rates to be higher than those *in situ*. However, the underlying mechanisms are the same.

Most of our experimental results confirm or are consistent with previous mesocosm studies of estuarine

and marine systems. As long as nutrients are replete, algae grow exponentially with tight coupling of carbon and nutrient flows, and little DOC accumulation (Banse 1994, Alldredge et al. 1995, Engel et al. 2002). After nitrogen depletion, carbon and nitrogen dynamics are decoupled, as reflected in changes in POC:PN ratios, the decline in chlorophyll *a* and accumulation of DOC (Engel et al. 2002, Van den Meersche et al. 2004). Nitrogen was never the limiting element in our study, and POC and PN dynamics remained tightly coupled. However, there was depletion of phosphate, which most probably caused the termination of the diatom bloom. The uncoupling of phosphor dynamics from those of carbon and nitrogen was reflected in the particulate C:N and C:P ratios. Van den Meersche et al. (2004) executed a similar, but shorter duration mesocosm experiment in a freshwater system, Randers Fjord, Denmark. The first 3 phases of our experiment can be compared to the 3 phases (growth, unbalanced growth and collapse) identified by Van den Meersche et al. (2004). However, in our experiment, phosphorus is the limiting nutrient instead of nitrogen in Randers Fjord. Also, by running the experiment a little longer, we were able to observe recovery of nutrient levels and initiation of a secondary bloom.

Phytoplankton–bacteria interactions and rate estimates

Heterotrophic bacteria are pivotal components of aquatic ecosystems. On the one hand, they recycle algal exudates and phytodetritus, and are thus part of the autotrophic food web. On the other hand, they process allochthonous organic material brought into the system from upstream and lateral inputs, and are thus part of the detrital food web. The tightness of the algal–bacterial link was assessed by administering ^{13}C-labeled bicarbonate. The observed delay between carbon fixation and bacterial response is consistent with many field observations of algal blooms (Ducklow 1999). A short overview of the estimated process rates and their interpretation follows. Algal exudates were a major subsidizer of bacterial growth, which is clear from the steep slope of bacterial $\delta^{13}C$. We can estimate the fraction of algal-derived DOC incorporated into bacterial biomass in 2 ways. Model II is a DOC uptake model based on the overflow model of phytoplankton extracellular release (Fogg 1983). In this model, DOC exudation correlates with primary production and is a mechanism to lose excess fixed carbon. Consequently, newly produced DOC has the same signature as DIC and the ratio $\delta^{13}C_{Bact}$:$\delta^{13}C_{DIC}$ will reflect the fraction of bacterial biomass originating from algal exudates. This ratio was found to be 58% at the end of the experiment. However, if one assumes heterotrophic mechanisms such as algal cell death, viral lysis (Bratbak et al. 1994, Murray & Eldridge 1994) and mesozooplankton sloppy feeding (Jumars et al. 1989) to be the main mechanisms for algal DOC release, new DOC will take on the algal signature rather than the DIC signature, and the final ratio $\delta^{13}C_{Bact}$:$\delta^{13}C_{algal}$ is an indicator for bacterial dependence on algal DOC. Under this scenario, the conclusion would be that 80% of bacterial carbon originated from algae grown in the mesocosm. A DOC uptake model would then result in higher DOC production rates and higher bacterial uptake rates compared to Model II. This second scenario involves viral lysis or sloppy zooplankton feeding for dissolved organic matter release and is consistent with the inferred accumulation of DON and DOP. Presumably, the real dependence of bacteria on algal dynamics is somewhat in between these 2 figures (58 to 80%). The high dependency of bacterial dynamics on algal products was already suggested by isotope natural abundances *in situ* (Boschker et al. 2005). The shift from upstream to downstream autochthonous support of bacterial growth can obviously be linked to the increased ratio of algae and algalderived material to imported carbon resources (Van den Meersche et al. 2009).

The DOC production rates by microplankton that we found were high (2 to 3 times higher than net biomass production); ~80% of the fixed carbon was channeled into DOC. Under the assumption that exudation is the main mechanism for DOC production, we can state that this is in the upper ranges of what has been reported in literature, with exudation varying between 0 and 80% of total primary production (Carlson 2002). A similarly high level of exudation was observed in a mesocosm study of river water entering Randers Fjord (Van den Meersche et al. 2004) and can be explained by the above-mentioned overflow mechanism, assuming that under nutrient stress, it is more efficient for algae to exudate the surplus of primary products (capsular material, carbohydrates) than to store them (Fogg 1983). Such high exudation values have also been found in oligotrophic coastal waters (Gonzalez et al. 2008) and in the North Sea, especially during bloom situations (Lancelot 1979, Lancelot & Billen 1984), but is not clear whether high rates of mucus secretion by *Phaeocystis* are available directly to bacteria.

Allochthonous and autochthonous contributions to mesozooplankton diet

The ^{13}C-bicarbonate labeling approach clearly highlighted the role of local primary production in supporting consumers, but estuarine plumes are also rich in allochthonous carbon from riverine and upper estuar-

ine sources. The role of external subsidies in mesozooplankton production in estuarine plumes is still unclear. Van den Meersche et al. (2009) used a combined natural abundance isotope-biomarker method to evidence the importance of allochthonous organic matter in upstream regions of a highly subsidized estuary like the Scheldt. However, the method used in that study is not applicable to the downstream regions because of overlap in isotopic signature of autochthonous and allochthonous carbon. Here we tackled this problem by adding inorganic ^{13}C, which labels only the autochthonous carbon. The steep gradient in isotope signatures created by using high labeling levels allowed us to observe subtle but rapid switches in mesozooplankton feeding behaviour. During the diatom bloom, algae were evidently available in excess, and selective grazing of mesozooplankton on algae could be identified. The fast switch from labeled to non-labeled food sources by *Temora longicornis* after Day 4 was somewhat surprising. Such opportunistic behaviour of copepods has been found over seasonal time-scales (Gentsch et al. 2009), but it is remarkable that it can also occur in short time-scale experiments such as this one.

The use of ^{13}C and ^{15}N as deliberate tracers revealed some other key observations on the functioning of mesozooplankton. First, there is the very rapid turnover in *Temora longicornis* carbon: after 4 d, >85% of its carbon came from primary production occurring during the experiment; this means that the zooplankton biomass is replaced at a rate of 50% d^{-1}. More striking though, is the rapid diet shift to non-labeled food sources after the bloom. *T. longicornis* either consumes detritus directly, or via bacteria and microzooplankton. In addition to the information obtained from the ^{13}C-bicarbonate labeling, the ^{13}C-glucose treatment provided evidence for mesozooplankton carbon acquisition via bacteria (and microzooplankton). In this treatment, incorporation of ^{13}C in *T. longicornis* was gradual and continued until the end of the experiment, while POC, heterotrophic bacteria and microzooplankton became strongly enriched in the first 2 d, subsequently diluted by primary production from a relatively low labeled DIC pool. This gradual and steady enrichment in the ^{13}C glucose treatment and the dilution of ^{13}C in the bicarbonate treatment after Day 4 both suggest that *T. longicornis* acquired part of its carbon via bacteria (and microzooplankton). *T. longicornis* is known as a herbivore, but capable of omnivory (Gentsch et al. 2009), consistent with our data.

The picture is different for *Centropages* sp., both in terms of its labeling levels and dynamics. *Centropages* was not identified up to species level, but most probably it was either *C. hamatus* or *C. typicus*, the 2 common species along the North Sea Coast (Durbin & Kane 2007). These species are known as omnivorous or carnivorous copepods (Calbet et al. 2007), consistent with our data showing rapid incorporation of ^{13}C added in the form of glucose, and delayed appearance of ^{13}C added in the form of bicarbonate.

Microzooplankton

It remains difficult to study microzooplankton grazing in natural communities. Laboratory experiments that measure grazing and growth of individual grazer species on different sources are useful, but given the large variety of species in the wild, many of whom are uncultivable, these laboratory experiments only involve a small number of microzooplankton taxa and remain far from the field situations where assemblages of microzooplankton graze upon a large variety of algae, bacteria and detritus. Estimation of grazing using the dilution method uses a community based approach, but has a set of problems of its own and may lead to ambiguous or imprecise rate estimates (Landry & Hassett 1982). The glucose labeling approach applied in this study has demonstrated transfer from bacteria to higher trophic levels, and turns out to be a valuable alternative, albeit with its own strengths and flaws. It can be applied to mesocosms with varying size or time scale, or *in situ* (Van Oevelen et al. 2006) without affecting ecosystem functioning. However, we cannot assume that heterotrophic bacteria are the only consumers of glucose and that all observed label uptake in eukaryotic PLFA comes from grazing on bacteria. Different groups of algae, and especially diatoms, have shown the ability to take up dissolved organic sources of carbon and nitrogen, most notably glucose (Droop 1957, Rivkin 1987, Antia et al. 1991, Radchenko et al. 2004). This means that the label uptake observed in eukaryotic lipids may very well be due to direct glucose uptake as well as grazing. Model III revealed that direct consumption of ^{13}C-glucose by microplankton was 5 times less than that incorporated via heterotrophic bacteria.

One may also wonder whether all branched fatty acids are associated to bacteria. While some heterotrophic flagellates and dinoflagellates have a proven ability to synthesize their own fatty acids (Klein Breteler et al. 1999, Vera et al. 2001), ciliates have been shown to incorporate the lipids of their food sources without major changes, including bacterial branched fatty acids (Ederington et al. 1995, Harvey et al. 1997, Klein Breteler et al. 2004). Heterotrophic flagellates can synthesize polyunsaturated fatty acids, most notably ω6 lipids, but these synthesizing abilities are very species-dependent and they still appear to incorporate bacterial branched fatty acids in variable proportions (Vera et

al. 2001). Thus, label uptake in branched fatty acids is due to synthesis by bacteria, but part of the observed branched fatty acids may already have been incorporated in microzooplankton biomass. Label uptake in polyunsaturated fatty acids may be due to direct uptake of glucose (Rossi et al. 2009), or microzooplankton grazing of bacteria and subsequent synthesis of polyunsaturated fatty acids. There is insufficient knowledge on these mechanisms to draw solid conclusions, and we therefore recommend experimental studies to address this issue and to explore novel methodologies to analyse the isotopic composition of single-celled organisms, such as nanoSIMS (Musat et al. 2008).

Model design

In this work, we opted to apply a set of simple, separately fitted models. This approach is much simpler than the all-encompassing ecosystem model that was used in Van den Meersche et al. (2004). There is an evident loss in predicting power if a model only considers a subsection of the ecosystem. The primary goal of the modeling presented here is to estimate ecosystem fluxes from the data that consist of biomasses and stable isotopic composition. This technique, also known as inverse modeling, can readily make use of sophisticated statistical techniques to assess the robustness of the estimates, something that is not yet possible for a more complicated model. Estimated parameters in our case include algal carbon fixation and exudation rates, bacterial production rate and zooplankton grazing rates during and after a mesocosm bloom. We used a Bayesian framework to estimate parameter uncertainty (Omlin & Reichert 1999), as implemented in the R package FME (Soetaert & Petzoldt 2010). The rather narrow uncertainty intervals in most fluxes demonstrate that it is possible to estimate process rates of the microbial food web in a mesocosm setup using stable isotopes, biomarkers and simplified models. However, under which conditions these results can be translated to the field is difficult to assess; it is likely that the responses in the mesocosms were quicker and more pronounced, and the obtained rates should therefore be assumed to be in the upper range of field values.

Acknowledgements. We thank P. van Rijswijk for experimental and laboratory support and M. Houtekamer and P. van Breugel for laboratory support and 3 anonymous referees for constructive feedback. C. Heip provided guidance and access to research facilities. The research was supported by grants from the Flemish Fund for Scientific Research (FWO) and the Netherlands Organisation for Scientific Research (NWO), and by extra funding from the University of Ghent. This is contribution 5000 from the Netherlands Institute of Ecology.

LITERATURE CITED

Alldredge AL, Gotschalk CC, Passow U, Riebesell U (1995) Mass aggregation of diatom blooms: insights from a mesocosm study. Deep-Sea Res II 42:9–27

Anderson TR, Williams PJLeB (1998) Modelling the seasonal cycle of dissolved organic carbon at station E1 in the English Channel. Estuar Coast Shelf Sci 46:93–109

Andersson MGI, Brion N, Middelburg JJ (2006) Comparison of nitrifier activity versus growth in a turbid, tidal estuary (Scheldt estuary in northern Europe). Aquat Microb Ecol 42:149–158

Antia NJ, Harrison PJ, Oliveira L (1991) The role of dissolved organic nitrogen in phytoplankton nutrition, cell biology and ecology. Phycologia 30:1–89

Banse K (1994) Uptake of inorganic carbon and nitrate by marine plankton and the Redfield ratio. Global Biogeochem Cycles 8:81–84

Berg GM, Glibert PM, Chen CC (1999) Dimension effects of enclosures on ecological processes in pelagic systems. Limnol Oceanogr 44:1331–1340

Billen G, Joiris C, Wijnant J, Gillain G (1980) Concentration and microbiological utilization of small organic molecules in the Scheldt estuary, the Belgian coastal zone of the North Sea and the English Channel. Estuar Coast Shelf Sci 11:279–294

Boschker HTS, Middelburg JJ (2002) Stable isotopes and biomarkers in microbial ecology. FEMS Microbiol Ecol 40: 85–95

Boschker HTS, de Brouwer JFC, Cappenberg TE (1999) The contribution of macrophyte-derived organic matter to microbial biomass in salt-marsh sediments: Stable carbon isotope analysis of microbial biomarkers. Limnol Oceanogr 44:309–319

Boschker HTS, Kromkamp JC, Middelburg JJ (2005) Biomarker and carbon isotopic constraints on bacterial and algal community structure and functioning in a turbid, tidal estuary. Limnol Oceanogr 50:70–80

Bratbak G, Thingstad F, Heldal M (1994) Viruses and the microbial loop. Microb Ecol 28:209–221

Brinch-Iversen J, King GM (1990) Effects of substrate concentration, growth state, and oxygen availability on relationships among bacterial carbon, nitrogen and phospholipid phosphorus content. FEMS Microbiol Lett 74:345–356

Calbet A, Carlotti F, Gaudy R (2007) The feeding ecology of the copepod *Centropages typicus* (Kroyer). Prog Oceanogr 72:137–150

Carlson CA (2002) Production and removal processes. In: Hansell DA, Carlson CA (eds) Biogeochemistry of marine dissolved organic matter. Academic Press, San Diego, CA, p 91–151

De Kluijver A, Soetaert K, Schulz KG, Riebesell U, Bellerby RGJ, Middelburg JJ (2010) Phytoplankton–bacteria coupling under elevated CO2 levels: a stable isotope labelling study. Biogeosciences 7:3783–3797

Droop MR (1957) Auxotrophy and organic compounds in the nutrition of marine phytoplankton. J Gen Microbiol 16: 229–231

Ducklow HW (1999) The bacterial component of the oceanic euphotic zone. FEMS Microbiol Ecol 30:1–10

Durbin E, Kane J (2007) Seasonal and spatial dynamics of *Centropages typicus* and *C. hamatus* in the western North Atlantic. Prog Oceanogr 72:249–258

Ederington MC, McManus GB, Harvey HR (1995) Trophic transfer of fatty-acids, sterols, and a triterpenoid alcohol between bacteria, a ciliate, and the copepod *Acartia tonsa*. Limnol Oceanogr 40:860–867

Engel A, Goldthwzit S, Passow U, Alldredge A (2002) Temporal decoupling of carbon and nitrogen dynamics in a mesocosm diatom bloom. Limnol Oceanogr 47:753–761

Evrard V, Soetaert K, Heip CHR, Huettel M, Xenopoulos MA, Middelburg JJ (2010) Carbon and nitrogen flows through the benthic food web of a photic subtidal sandy sediment. Mar Ecol Prog Ser 416:1–16

Fogg GE (1983) The ecological significance of extracellular products of phytoplankton photosynthesis. Bot Mar 26: 3–14

Gentsch E, Kreibich T, Hagen W, Niehoff B (2009) Dietary shifts in the copepod *Temora longicornis* during spring: evidence from stable isotope signatures, fatty acid biomarkers and feeding experiments. J Plankton Res 31:45–60

Gonzalez N, Gattuso JP, Middelburg JJ (2008) Oxygen production and carbon fixation in oligotrophic coastal bays and the relationship with gross and net primary production. Aquat Microb Ecol 52:119–130

Harvey HR, Ederington MC, McManus GB (1997) Lipid composition of the marine ciliates *Pleuronema* sp. and *Fabrea salina*: shifts in response to changes in diet. J Eukaryot Microbiol 44:189–193

Hayes JM (2001) Fractionation of carbon and hydrogen isotopes in biosynthetic processes. Rev Mineral Geochem 43: 225–277

Heip CHR, Goosen NK, Herman PMJ, Kromkamp J, Middelburg JJ, Soetaert S (1995) Production and consumption of biological particles in temperate tidal estuaries. Oceanogr Mar Biol Annu Rev 33:1–149

Jumars PA, Penry DL, Baross JA, Perry MJ, Frost BW (1989) Closing the microbial loop: dissolved carbon pathway to heterotrophic bacteria from incomplete ingestion, digestion and absorption in animals. Deep-Sea Res I 36:483–495

Klein Breteler WCM, Schogt N, Baas M, Schouten S, Kraay GW (1999) Trophic upgrading of food quality by protozoans enhancing copepod growth: role of essential lipids. Mar Biol 135(1):191–198

Klein Breteler WCM, Koski M, Rampen S (2004) Role of essential lipids in copepod nutrition: no evidence for trophic upgrading of food quality by a marine ciliate. Mar Ecol Prog Ser 274:199–208

Kromkamp J, Peene J, van Rijswijk P, Sandee A, Goosen N (1995) Nutrients, light and primary production by phytoplankton and microphytobenthos in the eutrophic, turbid Westerschelde estuary (The Netherlands). Hydrobiologia 311:9–19

Lancelot C (1979) Gross excretion rates of natural marine phytoplankton and heterotrophic uptake of excreted products in the Southern North Sea, as determined by short-term kinetics. Mar Ecol Prog Ser 1:179–186

Lancelot C, Billen G (1984) Activity of heterotrophic bacteria and its coupling to primary production during the spring phytoplankton bloom in the Southern Bight of the North Sea. Limnol Oceanogr 29:721–730

Landry MR, Hassett RP (1982) Estimating the grazing impact of marine microzooplankton. Mar Biol 67:283–288

Middelburg JJ, Barranguet C, Boschker HTS, Herman PMJ, Moens T, Heip CHR (2000) The fate of intertidal microphytobenthos carbon: an in situ ^{13}C-labeling study. Limnol Oceanogr 45:1224–1234

Moodley L, Boschker HTS, Middelburg JJ, Pel R, Herman PMJ, de Deckere E, Heip CHR (2000) Ecological significance of benthic foraminifera: ^{13}C labelling experiments. Mar Ecol Prog Ser 202:289–295

Murray AG, Eldridge PM (1994) Marine viral ecology: incorporation of bacteriophage into the microbial planktonic food-web paradigm. J Plankton Res 16:627–641

Musat N, Halm H, Winterholler B, Hoppe P and others (2008) A single-cell view on the ecophysiology of anaerobic phototrophic bacteria. Proc Natl Acad Sci USA 105: 17861–17866

Omlin M, Reichert P (1999) A comparison of techniques for the estimation of model prediction uncertainty. Ecol Model 115 (1):45–59

Pace MLS, Carpenter R, Cole JJ, Coloso JJ and others (2007) Does terrestrial organic carbon subsidize the planktonic food web in a clear-water lake? Limnol Oceanogr 52: 2177–2189

R Development Core Team (2010). R: a language and environment for statistical computing. R Foundation for Statistical Computing, Vienna, available at www.R-project.org/

Radchenko IG, Il'yash LV, Fedorov VD (2004) Effect of exogenous glucose on photosynthesis in the diatom *Thalassiosira weissflogii* depending on nitrate nitrogen supply and illumination. Biol Bull 31(1):67–74

Rivkin RB (1987) Heterotrophy and photoheterotrophy by antarctic microalgae: light-dependent incorporation of amino-acids and glucose. J Phycol 23:442–452

Rossi F, Vos M, Middelburg JJ (2009) Species identity, diversity and microbial carbon flow in reassembling macrobenthic communities. Oikos 118:503–512

Soetaert K, Petzoldt T (2010) Inverse modelling, sensitivity and Monte Carlo analysis in R using package FME. J Stat Softw 33:1–28

Soetaert K, Middelburg JJ, Heip CHR, Meire P, Van Damme S, Maris T (2006) Long-term change in dissolved inorganic nutrients in the heterotrophic Scheldt estuary (Belgium, The Netherlands). Limnol Oceanogr 51:409–423

Soetaert K, Petzoldt T, Setzer RW (2010) Solving differential equations in R: package deSolve. J Stat Softw 33:1–25

Tackx M, Irigoien X, Daro N, Castel J, Zhu L, Zhang X, Nijs J (1995) Copepod feeding in the Westerschelde and the Gironde. Hydrobiologia 311:71–83

Van den Meersche K, Middelburg JJ, Soetaert K, van Rijswijk P, Boschker HTS, Heip CHR (2004) Carbon–nitrogen coupling and algal–bacterial interactions during an experimental bloom: modeling a ^{13}C tracer experiment. Limnol Oceanogr 49:862–878

Van den Meersche K, van Rijswijk P, Soetaert K, Middelburg JJ (2009) Autochthonous and allochthonous contributions to mesozooplankton diet in a tidal river and estuary: integrating carbon isotope and fatty acid constraints. Limnol Oceanogr 54:62–74

Van Oevelen D, Moodley L, Soetaert K, Middelburg JJ (2006) The trophic significance of bacterial carbon in a marine intertidal sediment: results of an *in situ* stable isotope labeling study. Limnol Oceanogr 51:2349–2359

Vera A, Desvilettes C, Bec A, Bourdier G (2001) Fatty acid composition of freshwater heterotrophic flagellates: an

Appendix 1. Model equations

General description of model structure

The change of carbon concentration in a compartment X is described as:

$$\frac{dC_X}{dt} = \sum_{Sources} \text{Uptake} - \sum_{Sinks} \text{Loss} \quad (A1)$$

while the change in isotope composition is described as:

$$\frac{d\,\delta^{13}C_X}{dt} = \sum_{Sources} (\delta^{13}C_{Source} - \delta^{13}C_X) \times \frac{\text{Uptake}}{C_X} \quad (A2)$$

where C_X is expressed in µmol C l^{-1}, and uptakes and losses are expressed in µmol C l^{-1} d^{-1}. Note that the expression for change in isotope composition does not take into account fractionation; as the samples are highly enriched, fractionation can be neglected.

For independent variables, data are used as forcings in the model, while dependent variables are calculated and then fitted to existing data.

Model I: Primary production (PP)

Model I estimates autotrophic uptake (PP, µmol C l^{-1} d^{-1}) in eukaryotic microplankton, mainly composed of algae. Microplankton concentration (C_{MP}, µmol C l^{-1}) and isotope composition ($\delta^{13}C_{MP}$, ‰) are derived from eukaryote-specific polar lipid fatty acids (PLFA) in suspended matter. The model equations are:

$$\frac{d\,\delta^{13}C_{MP}}{dt} = (\delta^{13}C_{DIC} - \delta^{13}C_{MP}) \times \nu_{PP} \quad (A3)$$

$$PP = \nu_{PP} \times C_{MP} \quad (A4)$$

Independent variables: t, C_{MP} and $\delta^{13}C_{DIC}$.
Dependent variable: $\delta^{13}C_{MP}$.
Estimated parameter: ν_{PP}.

Model II: Bacterial uptake

This model aims to estimate exudation of labile DOC by algae (Ex) and its subsequent uptake by bacteria (HU_1) compared to uptake of other, non-labeled DOC (HU_2). Isotopic composition and concentration of eukaryotic and bacterial carbon are derived from PLFA in suspended matter.

$$\frac{d\,LabDOC}{dt} = Ex - HU_1 \quad (A5)$$

$$\frac{d\,\delta^{13}C_{LabDOC}}{dt} = (\delta^{13}C_{DIC} - \delta^{13}C_{LabDOC})\nu_{Ex} \quad (A6)$$

$$\frac{dC_{Bact}}{dt} = HU_1 + HU_2 \quad (A7)$$

$$\frac{d\,\delta^{13}C_{Bact}}{dt} = (\delta^{13}C_{LabDOC} - \delta^{13}C_{Bact})\frac{HU_1}{C_{Bact}} + (\delta^{13}C_{DOC} - \delta^{13}C_{Bact})\nu_{HU2}$$

$$Ex = \nu_{Ex} \times C_{MP}$$
$$HU_1 = \nu_{HU1} \times C_{Bact} \times \frac{LabDOC}{LabDOC + k_{HU1}}$$
$$HU_2 = \nu_{HU2} \times C_{Bact} \quad (A8)$$

Independent variables: C_{MP}, $\delta^{13}C_{DIC}$, $\delta^{13}C_{DOC}$.
Dependent variables: $LabDOC$, C_{Bact}, $\delta^{13}C_{LabDOC}$, $\delta^{13}C_{Bact}$.
Estimated parameters: ν_{Ex}, ν_{HU1}, ν_{HU2}, k_{HU1}.

Model III: Primary production, microplankton glucose uptake and microzooplankton grazing

This model addresses the different pathways for C uptake in eukaryotic microplankton: primary production, microzooplankton grazing on bacteria and direct uptake of glucose. Both the results from the DIC labeling and the glucose labeling are used in this model. $\delta^{13}C$ of DIC in the bicarbonate-labeled replicates (A,B) and $\delta^{13}C$ of bacteria in the glucose-labeled treatment (C) are used as independent variables, while $\delta^{13}C$ of DIC in the glucose-labeled treatment and $\delta^{13}C$ of MP (A, B and C) are the dependent variables.

$$\frac{d\,\delta^{13}C_{MP}}{dt} = (\delta^{13}C_{DIC} - \delta^{13}C_{MP})\nu_{PP} + (\delta^{13}C_{Bact} - \delta^{13}C_{MP})\frac{G}{C_{Bact}} + (\delta^{13}C_{Glu} - \delta^{13}C_{MP})\frac{MGU}{C_{MP}}\mu_{MP} \quad (A9)$$

$$\frac{d\,\delta^{13}C_{DIC}}{dt} = (\delta^{13}C_{Glu} - \delta^{13}C_{DIC})\frac{MGU}{DIC}(1-\mu_{MP}) + (\delta^{13}C_{Bact} - \delta^{13}C_{DIC})\frac{G}{DIC}(1-\mu_{MP}) + (\delta^{13}C_{Glu} - \delta^{13}C_{DIC})\frac{BGU}{DIC}(1-\mu_{Bact}) \quad (A10)$$

Primary production is linear to the concentration of microplankton, which is assumed to consist mostly of algae: $PP = \nu_{PP} \times C_{MP}$.

Glucose uptake by microplankton and bacteria include a Monod-type response to glucose concentration:

$$MGU = \nu_{GU} \times C_{MP} \times \frac{Glucose}{Glucose + k_{GU}} \quad (A11)$$

$$BGU = \nu_{BGU} \times C_{Bact} \times \frac{Glucose}{Glucose + k_{BGU}} \quad (A12)$$

Microzooplankton grazing on bacteria is a quadratic function of the bacterial concentration: $G = \nu_G \times (C_{Bact})^2$.

Independent variables: C_{MP}, DIC, C_{Bact}, $\delta^{13}C_{Bact}$, $Glucose$, $\delta^{13}C_{Glu}$. Dependent variables: $\delta^{13}C_{MP}$, $\delta^{13}C_{DIC}$.
Estimated parameters: ν_{PP}, ν_G, ν_{GU}, ν_{BGU}, k_{MGU}, k_{BGU}, and the respective growth efficiencies of microplankton and bacteria: μ_{MP} and μ_{Bact}.

Editorial responsibility: Antonio Bode, A Coruña, Spain

Submitted: October 12, 2010; Accepted: February 18, 2011
Proofs received from author(s): May 3, 2011